Defect Engineering with Group III Dopants in 2D Monolayer SiC for Improved Electronic Devices

Emmanuel Igumbor[a], Patience Ajeh[b], Edwin Mapasha[c], Ezekiel Omotoso[d], Abdulrafiu Raji[e,d]

[a] *Department of Mechanical Engineering Science, Faculty of Engineering and the Built Environment, University of Johannesburg, Johannesburg, South Africa*
[b] *Department of Theoretical and Applied Physics, African University of Science and Technology, Abuja 900107, Nigeria.*
[c] *Department of Physics, University of Pretoria, Pretoria 0002, South Africa.*
[d] *Department of Physics and Engineering Physics, Obafemi Awolowo University, Ile-Ife, 220005, Nigeria*
[e] *Center for Augmented Intelligence and Data Science, College of Science, Engineering and Technology, University of South Africa Florida 1709, South Africa*
[f] *National Institute of Theoretical and Computational Sciences (NITheCS), South Africa*

Abstract

Point defects in 2D monolayer SiC have played important roles in enhancing its performance for high-power electronic applications. Despite the fact that several point defects in 2D monolayer SiC have been reported, the impact of group III dopants has not been well understood. In this study, we employed hybrid density functional theory to investigate group III dopants (B, Al, Ga, In, and Tl) in 2D monolayer SiC. The B_C is the most energetically favorable, whereas Tl_C is the least favorable. At low temperature, the B_C exhibits high concentration, and the B_{Si} exhibits negligible concentration. The Ga_{Si} shows relatively low concentrations at 250–300 K and technologically significant levels at high temperature. The Ga_C is increas-

*Corresponding author
Email address: elgumuk@gmail.com (Emmanuel Igumbor)

ingly relevant at high temperatures and the Tl_C and Tl_{Si} show vanishingly small concentrations up to $\sim$ 800 K, with only minor activation at high temperature. Group III dopants substituted at the C-sites generally induce mid-gap states, with their Fermi levels located near the middle of the band gap. In contrast, when substituted at the Si sites, these dopants do not induce mid-gap states. Instead, the dopant-induced states close to the Fermi level, leading to *p*-type behavior. Moreover, C-site substitution often induces local magnetic moments and breaks spin symmetry between the spin-up and spin-down states, whereas Si-site substitution result in symmetric, non-magnetic behavior. This study provides theoretical insights into the potential use of group III dopants in 2D monolayer SiC as a means to modify its electronic and magnetic properties for applications in nano- and microelectronic devices that can operate in high-temperature and harsh environments.
Keywords: Dopant, formation energy, charge transfer, magnetic moment, density of states, defect concentration

---

1. Introduction

Bulk SiC is a semiconductor with many known polytypes [1]. Among the widely studied polytypes are 2C, 3C, 4H and 6H [1, 2, 3, 4]. The 2C, 3C, 4H, and 6H have received significant attention due to their relatively wide band gaps compared to other polytypes [5]. The thermal, electronic, optical, structural and spectroscopic properties of the 2C, 3C, 4H, and 6H bulk SiC polytypes have been extensively reported in numerous studies [1, 3, 4, 6, 7]. Compared to other structural materials, Si, and wide band-gap semiconductors, SiC exhibits low density and thermal expansion coefficient,

high thermal conductivity and mechanical strength, a high elastic modulus with resistance to creep deformation and excellent chemical stability [1, 8]. Although SiC has long been known in its bulk form, it has recently been synthesized in a layer form [9, 10].

Since the discovery of graphene, a gapless layered material with remarkable electronic and mechanical properties, there has been growing interest in exploring other two-dimensional (2D) materials, such as MoS_2, WS_2, TiS_3 and WTe_2, among others. [11, 12, 13, 14, 15]. Many of these layered materials exhibit hexagonal honeycomb crystal structures [16, 17, 18, 19, 20, 21, 22, 23, 24]. Similarly to its bulk counterpart, 2D SiC exhibits a wide band gap of 2.54-3.26 eV [10, 25, 26, 27] making it a promising candidate for applications in power electronics, optoelectronics and devices operating under harsh environmental conditions [27]. Since the synthesis of 2D monolayer SiC, several studies have been conducted. Recent experimental investigations into its mechanical properties have confirmed the structural stability of 2D monolayer SiC [28].

The study of point defects is receiving increasing attention due to their ability to modify the intrinsic properties of semiconductors, thereby enhancing their performance [29, 6, 7, 30]. Several types of point defects have been reported in bulk SiC [2, 6, 7, 31, 32, 33, 34]. The insights gained from studying various semiconductors with defects are enormous. For example, point defects are used to adjust the band gap, enhance electrical conductivity, and control electron-hole interactions in semiconductors [2, 34, 35]. However, caution must be taken when introducing point defects in semiconductor, as they may lead to deep-level defects and create recombination centers due

to the presence of mid-gap states [2, 31, 34]. Therefore, it is important to understand the influence of point defects in semiconductors.

Group III dopants are important point defects commonly used to achieve *p*-type conductivity in semiconductors [36, 37]. Elements such as boron, aluminum, gallium and indium have been extensively used to dope semiconductors (silicon (Si) [38], germanium (Ge) [39, 40], silicon carbide (SiC) [41, 42], gallium nitride (GaN) [43]), due to their ability to act as electron acceptors. Several studies on point defects in bulk SiC have been reported [1, 3, 4, 6, 7, 31, 32]. In particular, the B atom has been shown to be energetically favorable at both Si and C sites, although its stability strongly depends on the growth conditions and temperature [41]. SiC can be efficiently doped to exhibit both n-type and p-type conductivity [41]. For example, doping of 3C-, 2H-, 4H- and 6H-SiC with n- and p-type materials leads to shifts of energy levels in both the conduction and valence band regions [44]. Gong *et al.* reported that doping SiC with group III elements enhances its photoelectric performance by improving carrier scattering mechanisms [45]. In addition, when silicon carbide nanotubes (SiCNTs) are doped with group III elements, their electrical conductivity exhibits a temperature-dependent behavior. Specifically, the conductivity tends to decrease as the temperature is elevated above 200 K [45]. Analysis of the absorption behavior of Al, In, and Ga in SiC indicates that these dopants preferentially occupy Si sites, exhibiting greater energetic stability at these positions [46]. The optical properties of SiC nanotubes (SiCNTs) doped with B, Al, Ga and In have also been investigated. In the wavelength range of 250–620 nm, the absorption peak of the dopants on the C-cites was found to be broad and low in intensity, while

that of the dopants on Si-cites was sharp and high in intensity [36]. These findings suggest that doping SiCNTs with B, Al, Ga and In can significantly enhance its potential for use in photodetection and photosensitive semiconductor devices [36]. Incorporation of dopants B, Al, Ga, and In has been shown to improve the electronic properties of semiconductors such as Ge, Si, and SiC [47, 48, 49]. However, improper incorporation of B, Al, In, and Ga can negatively affect semiconductor performance if not properly controlled at different temperatures. In the case of 2D monolayer SiC, the impact of these dopants on the structural, electronic and magnetic properties of the material remains largely unexplored. Furthermore, the concentration of the B, Al, In, and Ga dopants in 2D monolayer SiC at low and high temperature are still not well understood.

In this study, we used hybrid density functional theory to calculate the electronic, magnetic, and charge transfer properties of group III dopants (B, Al, In, and Ga) in 2D monolayer SiC. The concentrations of the defective systems at low to high temperatures were examined. The introduction of group III dopants into 2D monolayer SiC distorted its crystallinity. The formation energies of B, Al, In, and Ga dopants in 2D monolayer SiC are relatively low. Although Al atoms consistently act as donors regardless of the substitution site, the B, Ga, In, and Tl dopants tend to gain electrons from neighboring host atoms. When substituted at C sites, the B, Al, In, and Ga dopants induced magnetic moments in the 2D monolayer SiC lattice. The findings of this study are significant, as they offer valuable insights into the synthesis of doped 2D monolayer SiC for applications in high-power, high-temperature modern electronic devices.

2. Computational Details

DFT simulations of the structural, electronic, and magnetic properties of group III dopants in a 2D monolayer SiC were performed using the Vienna Ab initio Simulation Package (VASP). The projector augmented-wave method pseudopotential was used to effectively separate the chemically active valence electrons from the core electrons [50]. The Perdew-Burke-Ernzerhof functional within the generalized gradient approximation (GGA) was used for the exchange–correlation [51]. However, to achieve improved electronic properties, the hybrid functional of Heyd–Scuseria–Ernzerhof (HSE06) was employed [52]. For the HSE06 functional, we used a mixing parameter of 25% and a screening parameter of 0.2 $Å^{-1}$. To perform defect simulations, a 6×6×1 supercell containing 72 atoms was constructed from the relaxed unit cell of the 2D monolayer SiC . The relaxed lattice constants of the unit cell were $a = b = 3.08$ Å, which is in agreement with previous studies [53, 54]. The out-of-plane lattice constant was set to $c = 20$ Å, which is a vacuum layer introduced to prevent interlayer interactions due to periodic boundary conditions. The Brillouin zone of the supercell was sampled using a Monkhorst–Pack k-point grid of 4×4×1. The energy cut-off was set to 400 eV. The total energy convergence criterion was set to 10^{-6} eV, and the atomic forces acting on the atoms were relaxed until they were less than 0.001 eV/Å. Group III impurities were subsequently substituted into the relaxed supercell, either at Si or C lattice sites, and structural relaxation was carried out. The density of states (DOS) was calculated using a denser k-point grid. Bader analysis was performed to evaluate the electron charge transfer.

The defect concentration ($Defect_{\mathrm{C}}$) under equilibrium conditions is a

function of the formation energy E^{form}, and is given as;

$$Defect_{\text{C}} = N_{(\text{defect}-\text{sites})} \times \exp\left(-\frac{E^{\text{form}}}{k_B T}\right), \quad (1)$$

where $N_{\text{defect}-\text{sites}}$ is the possible number of sites that a defect can occupy, k_B is the Boltzmann constant and T is the temperature in Kelvin. The formation of defects is essential to determine whether a particular defect can form with favorable energy. Therefore, the formation energies of group III dopants in the 2D monolayer SiC were calculated as

$$E^{\text{form}} = E^{\text{defect}}_{\text{total}} - E^{\text{pristine}}_{\text{total}} + \mu_i^{\text{host}} - \mu_k^{\text{dopant}} \quad (2)$$

where $\text{E}^{\text{defect}}_{\text{total}}$, and $\text{E}^{\text{pristine}}_{\text{total}}$, are the total energy of the defective and pristine systems, respectively. The μ^{host} and μ^{dopant} are the chemical potential of the host atoms of type *ith* and the dopants of type *kth*. The chemical potentials of the group III atoms were calculated on the basis of their most stable elemental phases, using the energy per atom. However, for the chemical potentials of Si and C, we derived them from the formation enthalpy of SiC ($\Delta H^{\text{f}}(\text{SiC})$), calculated as

$$\Delta H^{\text{f}}(\text{SiC}) = \mu^{\text{bulk}}_{\text{Si}} + \mu^{\text{bulk}}_{\text{C}} - \mu^{\text{bulk}}_{\text{SiC}}, \quad (3)$$

where $\mu^{\text{bulk}}_{\text{Si}}$ and $\mu^{\text{bulk}}_{\text{C}}$ are the chemical potentials of bulk Si and C, respectively. The $\mu^{\text{bulk}}_{\text{SiC}}$ is the total energy per formula unit of bulk SiC used as a reference for equilibrium. However, the chemical potentials of Si (μ_{Si}) C (μ_{C}) must be carefully calculated to avoid the formation of secondary phases, which could lead to thermodynamic instability. Therefore, appropriate constraints should be applied as $\mu_{\text{Si}} + \mu_{\text{C}} = \mu^{\text{bulk}}_{\text{SiC}}$. To avoid pre-

cipitation of elemental Si or C, the following conditions must be imposed as $\mu_{\text{Si}} \leq \mu_{\text{Si}}^{\text{bulk}}$ and $\mu_{\text{C}} \leq \mu_{\text{C}}^{\text{bulk}}$. Hence, for Si-rich (C-poor) conditions ($\mu_{\text{Si}} = \mu_{\text{Si}}^{\text{bulk}}$), the $\mu_{\text{C}} = \mu_{\text{SiC}}^{\text{bulk}} - \mu_{\text{Si}}^{\text{bulk}}$. For the C-rich (Si-poor) conditions ($\mu_{\text{C}} = \mu_{\text{C}}^{\text{bulk}}$) the $\mu_{\text{Si}} = \mu_{\text{SiC}}^{\text{bulk}} - \mu_{\text{C}}^{\text{bulk}}$

3. Results and Discussion

3.1. Structural Properties of Group III Dopants in 2D Monolayer SiC

Table 1 lists the bond lengths between the impurity atoms and their nearest-neighbor host atoms. Figure 1 displays the relaxed geometry of the pristine 2D monolayer SiC, B_{Si} and Al_{C}. The relaxed pristine S-C bond length is 1.79 Å, which is in close agreement with previous studies [55, 56].

Table 1: The bond length between impurity (X) atoms and their nearest neighbour C or Si atom in Å.

X_{C}	X-Si	X_{Si}	X-C
B_{C}	1.93	B_{Si}	1.64
Al_{C}	2.21	Al_{Si}	1.93
Ga_{C}	2.19	Ga_{Si}	1.96
In_{C}	2.31	In_{Si}	2.11
Tl_{C}	2.32	Tl_{Si}	2.18

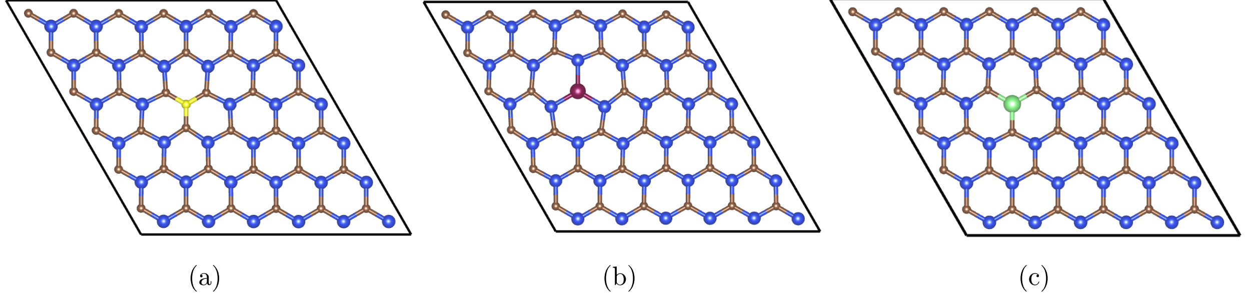

Figure 1: The relaxed geometry structures of the (a) Pristine 2D monolayer SiC (b) B_{Si}, and (c) Al_C. The blue, brown, purple and green spheres represent the Si, C, B and Al atoms, respectively.

.

The bond length increases down the group from B to Tl, as listed in Table 1. The B_{Si} formed the shortest bond (1.64 Å), indicating strong bonding. In contrast, the Tl and In atoms at either site (C or Si) introduce bond lengths exceeding 2.1 Å. The Tl-Si and Tl-C bonds exhibit greater lattice distortion due to the large atomic radius mismatch between Tl and the host atoms (Si or C). This mismatch introduces significant lattice distortion, which alter defect energetics as will be discussed later. The differences between the relaxed pristine Si-C bond and the X-Si bonds are 0.17, 0.42, 0.40, 0.52, and 0.53 Å, for B, Al, Ga, In, and Tl, respectively. However, the deviations in bond lengths between Si-C and X–C are relatively smaller than those of the X–Si bonds. For instance, the B-C, Al-C, Ga-C, In-C, and Tl-C bonds are shorter than the relaxed pristine Si-C bond by 0.15, 0.14, 0.17, 0.32, and 0.39 Å, respectively. The shorter X-C bonds (from Si-site doping) compared to X–Si bonds (from C-site doping) arise from the smaller size and higher electronegativity of C. This enhances bond strength, influ-

encing defect stability, lattice distortion, and electronic structure, thereby playing a critical role in tailoring the properties of 2D monolayer SiC for device applications. While we have not explicitly studied electronic potential constants and mechanical strain, previous studies have shown that lattice mismatch, particularly the substitution of a large dopant for a smaller atom, can induce significant strain [57, 58]. Furthermore, this strain can increase defect formation energy [59, 60]. In another report, it was argued that the introduction of such strain renders the formation of the dopant energetically unfavorable [61]. Therefore, in our study, the relatively large bond distances compared to those in pristine Si–C could induce strong lattice distortion and impact the formation energy.

3.2. Formation Energy of Group III Dopants in 2D Monolayer SiC

The formation energies of group III dopants in 2D monolayer SiC, substituted at either on the C or Si lattice sites, as a function of the chemical potential varying between the C-rich and Si-rich limits, are shown in Figure 2. The C-rich and Si-rich conditions define the allowable range of chemical potentials for 2D monolayer SiC. The intersection of the formation-energy curves indicates the chemical potential at which each dopant's preferred substitution site changes. If the formation energy lies below the intersection toward the C-rich side, the dopant is more energetically favorable at the C site. In contrast, above the intersection, toward the Si-rich limit, the Si site becomes more energetically favorable. Each crossing point in Figure 2 represents a stability boundary that marks where X_{C} and X_{Si} defects become thermodynamically competitive. As shown in Figure 2, the dopant site preference is tunable through growth conditions, and different defect configurations may

coexist near this boundary.

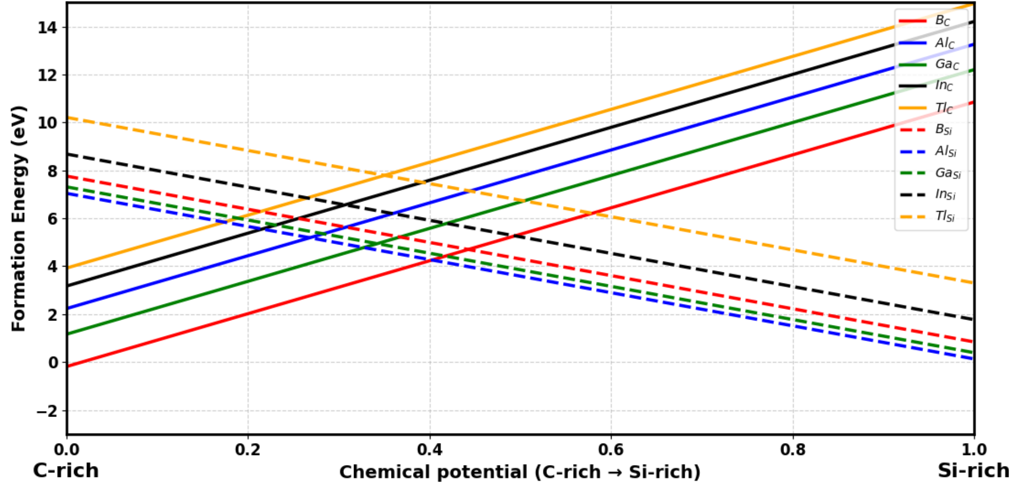

Figure 2: Formation energy phase diagram of group-III dopants in 2D monolayer SiC as a function of normalized chemical potential (0 = C-rich, 1 = Si-rich). Solid lines indicate C-site substitution, and dashed lines indicate Si-site substitution. All energies are in eV

.

Table 2 displays the formation energies of the substitutional dopants in 2D monolayer SiC under C–rich (Si–poor) and Si–rich (C–poor) chemical potential growth conditions. The B dopant is more energetically favorable at the C site under C-rich conditions. For instance, the formation energy of B_C is 0.19 eV, representing a significant improvement compared to Ref. [55], where a value of 4.00 eV was reported under applied strain. As reported in Ref. [55], the explicit inclusion of strain in the 2D monolayer SiC leads to an elevated formation energy of the B_C defect, in contrast to the present results, where the effect of strain on formation was not considered. The B_C and B_{Si} dopants are more spontaneous in their formation in 2D monolayer

SiC under C-rich and Si-rich growth conditions, respectively. The B_C with relatively low formation energy can be incorporated under moderate growth conditions. In SiC nanotubes, the formation energy of B_C (3.43 to 3.77 eV) [62] is higher, whereas that of B_{Si} (-0.54 to -0.26 eV) is lower compared to the 2D monolayer SiC. Under Si-rich growth conditions, Al, Ga, In, and Tl dopants are more energetically favorable when substituted on the Si lattice site. However, under C-rich (Si-poor) conditions, Al, Ga, In, and Tl are less energetically favorable.

Table 2: The formation energy (E^{form}) in eV of group III dopant (X) at C and Si sites in 2D monolayer SiC under C-rich and Si-rich conditions.

X_C			X_{Si}		
	C-rich	Si-rich		C-rich	Si-rich
B_C	-0.19	10.85	B_{Si}	7.76	0.84
Al_C	2.23	13.26	Al_{Si}	7.04	0.13
Ga_C	1.16	12.20	Ga_{Si}	7.31	0.39
In_C	3.17	14.21	In_{Si}	8.68	1.77
Tl_C	3.92	14.96	Tl_{Si}	10.21	3.30

The Al_{Si} dopant under Si-rich conditions is more energetically favorable; however, its formation energy is 0.26 eV lower than that of Ga_{Si} under the same Si-rich chemical potential conditions, which also remains energetically favorable. A similar behavior has been reported in bulk SiC [63], 4H-SiC [63] where Al is also more energetically favorable at the Si site. However, the formation energy of Al_C in 2D monolayer SiC is lower than that of the 4H-SiC[63]. The formation energy of Al_{Si} (0.12 eV) is relatively lower than the

value of approximately 0.90 eV reported in Ref. [56]. The Al dopant improved stability and increased the likelihood of incorporation on the Si site during material growth, which may improve device performance. The least stable dopant is the Tl when substituted at the C site. The formation energy increases down the group. implying that larger atoms (In, Tl) are energetically less favorable as dopants in 2D monolayer SiC. In all, While X_C is the most energetically favorable under C-rich chemical potential, X_{Si} is the most energetically favorable under Si-rich chemical potential conditions. From this point and further, the discussion will focus exclusively on dopants under their most energetically favorable chemical growth conditions; unfavorable conditions will not be further considered.

3.3. Defect Concentrations

In bulk SiC, defect evolution and stability have been extensively studied [7]. High-temperature annealing has been used to gain a deeper understanding of deep-level defects [7, 31]. The equilibrium defect concentration equation (Equation 1) was used to calculate the defect concentrations of group III dopants in 2D monolayer SiC. In this study, we used the calculated formation energies to determine the concentrations of group III dopants in a 2D monolayer SiC over a temperature range of 250 to 1500 K. The plots of the defect concentrations are shown in Figure 3.

The B_C defect exhibits a high defect concentration at 250 K. However, as the temperature increases, the concentration of B_C decreases exponentially, as shown in Figure 3a. When the temperature is between 600–1000 K, the concentration of the B_C shows steady decline at a slower rate. This shows that the B_C is exothermic and thermodynamically favorable at lower temper-

atures. Furthermore, at 1500 K, the defect concentration of B_C drops. The concentration of the B_{Si} at 250 K is $\sim$2.80 10^{-2} cm^{-2} (see Figure 3c). As the temperature increases to 600 K, the defect concentration of the B_{Si} rises to around 2.11×10^8 cm^{-2}. Increasing the temperature to 1500 K, the B_{Si} concentration increases significantly to 3.61×10^{12} cm^{-2}. This suggests that the B_{Si} can become active during high-temperature (600-1500 K) annealing. This maximizes the potential of the B_{Si} to be considered as an effective p-type dopant in 2D monolayer SiC, and provides guidance for high-temperature processing. In contrast to the B_C, the B_{Si} is endothermic, with significant defect concentrations emerging only at elevated temperatures.

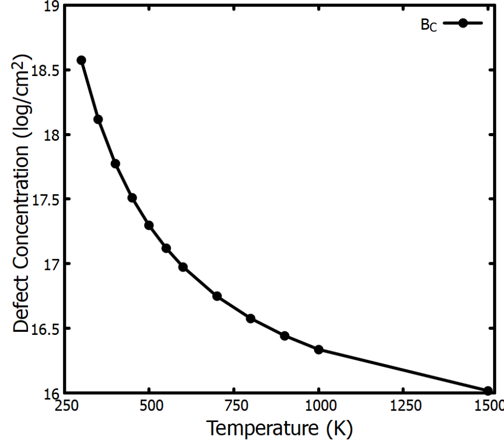

(a)

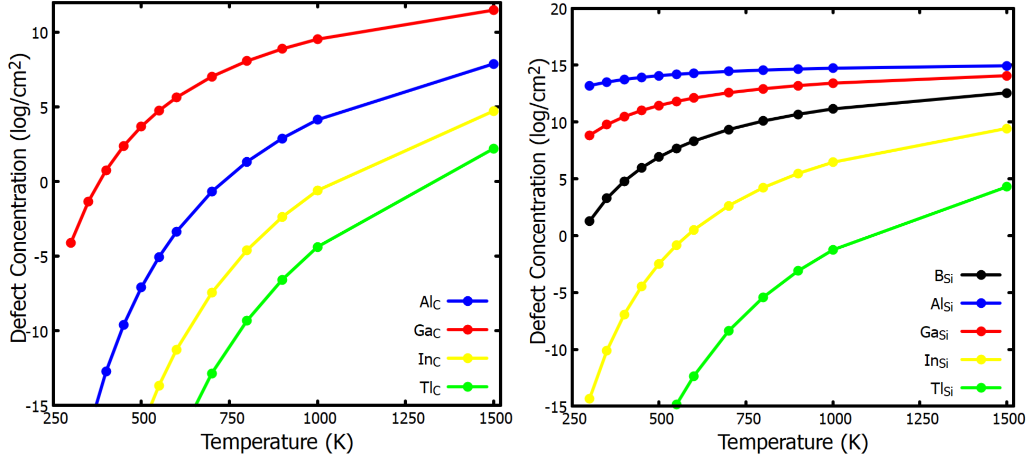

(b)

(c)

Figure 3: Defect concentrations of group III dopants in monolayer 2D SiC; (a) B_C, (b) dopants on C lattice site and (b) dopants on Si lattice site.

In bulk 4H–SiC and 6H–SiC, studies have shown that the B typically substitutes on the C-site. Furthermore, its concentrations is up to $\sim 10^{18}$–10^{20} cm^{-3} under doping conditions [64, 65, 66]. Whereas the B_{Si} is less favorable in bulk SiC due to size mismatch, unless grown under high-temperature or

non-equilibrium conditions. In this study, the results of the B_C which is dominant at low temperatures and that of the B_{Si} which only becomes relevant at high temperature, is consistent with the trend observed for that of the bulk 4H–SiC and 6H–SiC [64, 65, 66].

The Al_C has a low defect concentration throughout the temperature range (250-1200 K) (see Figure 3b). As the temperature increases from 250 to 500 K, the concentration of the Al_C is $\sim 7.97\times10^{-8}$ cm^{-2} at 500 K. Furthermore, at 1500 K, the concentration reaches $\sim 7.71\times10^{7}$ cm^{-2}. This is a significant increase compared to temperatures between 250–1200 K. Although the concentration of the Al_C remains relatively low, however, at 1500 K, it approaches typical dopant levels. This suggests that high-temperature processing could enable some incorporation of Al at C-site, potentially contributing to defect-assisted doping. However, given its lower stability compared to the Al_{Si}, the Al_C remains less favorable as a primary dopant in 2D monolayer SiC. The defect concentration of the Al_{Si} increases moderately with temperature. The Al_{Si} exhibits a strong temperature dependence characteristic of thermally activated processes. For example, as the temperature increases, the defect concentration of Al_{Si} increases exponentially, as shown in Figure 3c. The Al_{Si} concentration is $\sim 5.75\times10^{12}$ cm^{-2} at 250 K. This shows that a significant fraction of Si sites can be occupied by Al atoms in thermal equilibrium. Furthermore, as the temperature is elevated from 600 K to 1000 K, the Al_{Si} concentration continues to increase, howbeit at a slightly slower rate. At 600 K, the concentration of the Al_{Si} reaches 1.94×10^{14} cm^{-2}. This saturation-like behavior suggests that the defect formation may approach a limit dictated by available lattice sites or solubility constraints. Furthermore,

at high temperature (1500 K), we observed that the concentration of Al_{Si} is at its peaks (8.78×10^{14} cm^{-2}). The Al is likely to substitute Si-sites efficiently even at elevated temperatures, leading to the achievement of a *p*-type doping in 2D monolayer SiC [67]. However, care must be taken because at increasingly high temperature, there may be an introduction of scattering centers as well as trap states by the excessive Al_{Si} if not controlled. Therefore, thermal processing steps must be carefully controlled to avoid excess doping [68]. A comparison of this study with that of the bulk 4H–SiC and 6H–SiC shows some similarities. For instance, in bulk 4H–SiC and 6H–SiC, Al_{Si} in contrast to Al_C is more energetically favorable and it acts as a shallow acceptor as well as an efficient *p*-type dopant [69, 70, 71]. This is consistent with the result of this study where the Al_{Si} exhibits significantly higher concentrations across the temperature range compared to that of the Al_C. Furthermore, the Al_C shows much lower stability and concentration in both bulk and 2D cases, only reaching meaningful levels under high-temperatures (above 1200 K). As observed in bulk 4H–SiC and 6H–SiC, the incorporation of Al at C-sites remain minimal unless promoted by non-equilibrium or high-temperature processing [68, 72]. Therefore, both in bulk SiC and 2D monlayer SiC, Al_{Si} emerges as the more energetically favorable and responsible for *p*-type doping, while Al_C remains only relevant under extreme growth or annealing conditions.

At low temperatures ($\leq$ 300 K), the Ga_C defect concentration is negligible. As an example, between 250–350 K, the concentration of Ga_C is around $\sim 10^{-9}$ to $\sim 10^{-2}$ cm^{-2}. This suggests that the Ga_C is practically absent and has negligible impact on material properties. As temperature increases above

400 K, the concentration of the Ga_C reaches $\sim 2.44 \times 10^2$ cm4.32×10^5 cm^{-2} at 600 K. This rise strongly shows the presence of strong thermal activation on the Ga_C. At higher temperatures between 700–1000 K, Ga_C concentrations grow to significant levels ($\sim$ 10^7–10^9 cm^{-2}), suggesting that thermal activation strongly favors the defect formation. At elevated temperature of 1500 K, the concentration of the Ga_C reaches $\sim$ 3.04×10^{11} cm^{-2}. This suggests that the Ga_C could significantly influence electrical behavior. The Ga_C shows strong temperature dependence, but precise control over its concentration and distribution is essential to prevent unwanted compensation effects or defect clustering at high temperatures. As shown in Figure 3c, the Ga_{Si} exhibits a low concentration (below 10^7 cm^{-2}) at 250 K. This suggests negligible electronic or structural impact. However, as the temperature increases, the concentration of Ga_{Si} rises continuously. For example, at room temperature (300 K), the concentration of the Ga_{Si} is $\sim 10^9$ cm^{-2}, and at 600 K it reaches $\sim 10^{12}$ cm^{-2}. This is a strong evidence that the Ga_{Si} in 2D monolayer SiC can be effective at moderate processing increasing temperatures. Furthermore, between 700 K and 1000 K, the Ga_{Si} concentration increases rapidly. This implies that the Ga_{Si} is thermodynamically favorable at elevated temperatures. This makes Ga_{Si} a significant defect species during high temperature synthesis, where defect-mediated properties such as *p*-type conductivity are enhanced. As observed for the Al_{Si}, the Ga_{Si} may also contribute to defect clustering at 1500 K due to its high concentration. For instance, at 600–1500 K, the concentration of Ga_{Si} reach technologically significant levels ($> 10^{12}$–10^{14} cm^{-2}), which could influence material properties. The behavior of the Ga_{Si} is consistent with defect formation driven

by thermal activation. In bulk SiC, Ga substitutes preferentially at the Si site and acts as an acceptor [73, 74]. The Reported concentrations in bulk doping experiments is $\sim 10^{17}$–10^{19} cm^{-3} [74, 75]. However, the Ga_C is rare in bulk due to its poor stability. Our present results are consistent with the trend of Ga doped bulk SiC where the Ga_{Si} is strongly favored and thermally activated, while Ga_C remains negligible until very high temperatures.

The In_C defect exhibits a low concentration across the entire temperature range up to 1000 K. Even at 1500 K, its concentration remains around 10^4 cm^{-2}, indicating that the In_C may not spontaneously form under equilibrium conditions. This behavior is consistent with the significant size mismatch between In and C atom. However, under non-equilibrium conditions, such as ion implantation, irradiation, ion-beam synthesis, or plasma environments, there is a possibility that In_C may still form and be observable in 2D monolayer SiC. In contrast, the In_{Si} defect shows a strong temperature-dependent behavior, with its concentration increasing exponentially with temperature. At room temperature (300 K), the concentration is extremely low, below ($\sim 10^{-1}$ cm^{-2}). However, at 800 K, the concentration of the In_{Si} increases to $\sim 10^4$ cm^{-2}. Although still relatively low, this represents a significant rise. At 1500 K, the concentration of the In_{Si} reaches $\sim 10^9$ cm^{-2}, suggesting that this defect could become relevant under elevated temperature. For bulk 4H–SiC and 6H–SiC, reports show that In atom incorporation is difficult. Experimental studies show that the solubility of In atom is extremely low ($< 10^{13}$ cm^{-3}) under equilibrium conditions [76]. This findings are consistent with this present study where In_C is negligible, while In_{Si} becomes relevant only at very high temperatures. Furthermore, in the bulk 4H–SiC and 6H–

SiC, In atom tends to occupy Si sites under extreme growth conditions, but the resulting concentrations are still orders of magnitude lower than those of B or Ga [77].

The Tl_C has low defect concentrations at low temperatures. For instance between 400-800 K, the concentration of the Tl_Cm is almost zero. This shows that the Tl_C is practically non-existent under equilibrium conditions even up to 800 K. This could be attributed to the large atomic size mismatch between Tl and C. As the temperature is elevated beyond 1000 K, the concentration of the Tl_C increased to $\sim 10^{-5}$ cm^{-2}. The concentration of the Tl_C becomes substantial at 1500 K ($\sim 1.61 \times 10^{2}$ cm^{-2}). This trend suggests that the Tl_C is strongly thermally activated. That is the Tl_C may only form in measurable quantities under high-temperature conditions or non-equilibrium processing, such as ion implantation or plasma-assisted growth. The Tl_{Si} defect shows negligible concentrations at low temperatures. For instance, the concentration of the Tl_{Si} is $\sim 10^{-6}$ cm^{-2} at 800 K. This suggests that the Tl_{Si} is extremely unlikely to form spontaneously under equilibrium conditions. As in the case of Tl_C, the Tl_{Si} behavior is consistent with the significant size and mismatch between Tl and Si. As temperature increases, the concentration of the Tl_{Si} rises. For example, at 900 K, the concentration of the Tl_{Si} is $\sim 8.00 \times 10^{-4}$ cm^{-2}. The defect becomes more significant at higher temperatures. For instance, at 1000 K, the concentration of the Tl_{Si} rises to ~ 5.60 cm^{-2}, and at 1500 K, it reaches $\sim 1.96 \times 10^{4}$ cm^{-2}, indicating that the defect could significantly influence material properties at very high temperatures. In this study, it is important to note that the predicted high- or low-temperature concentrations of group-III substitutions in 2D monolayer

SiC are purely theoretical estimates obtained from thermodynamic defect statistics. Since no experimental measurements of group-III dopant concentrations in 2D monolayer SiC have been reported, these predictions may serve as useful information for future molecular beam epitaxy–grown-grown or chemical vapor deposition-grown samples.

3.4. Partial Density of States of Dopants in Monolayer 2D SiC

To provide insights into how the dopant influences the electronic properties of 2D monolayer SiC, the partial density of states (PDOS) of all defective systems were studied. Figure 4 displays the plot of the PDOS of the B, Al, Ga, In and Tl dopants in 2D monolayer SiC. The PDOS of the pristine 2D monolayer SiC shows similar behavior with already existing results in the literature [56, 78]. For example, the Fermi level of the pristine system is pinned to the valence band maximum (VBM). This shows that the 2D monolayer SiC is a *p*-type semiconductor. The PDOS for B_{Si} did not induce any significant mid-gap state as shown in Fig 4b. The Fermi level is pinned directly to the VBM. The *p* orbitals of C, B, and Si atoms induce states near their Fermi level. The B_{Si} slightly reduces the band gap of the host 2D monolayer SiC by approximately 0.20 eV. In the PDOS, the B_C defect introduces mid-gap states originating mainly from the *p* orbitals of B and C atoms. Strong orbital hybridization results in significant overlap of these orbitals. The Fermi level is pinned to the valence band, which is dominated by *p* orbitals of B and C, while the conduction band minimum (CBM) remains weakly populated. The CBM of B_C is primarily populated by the *p* orbitals of Si. The induced mid-gap states are highly asymmetric, suggesting spin polarization. This behavior is promising for spin-dependent device applications and further

reduces the band gap of the host 2D monolayer SiC.

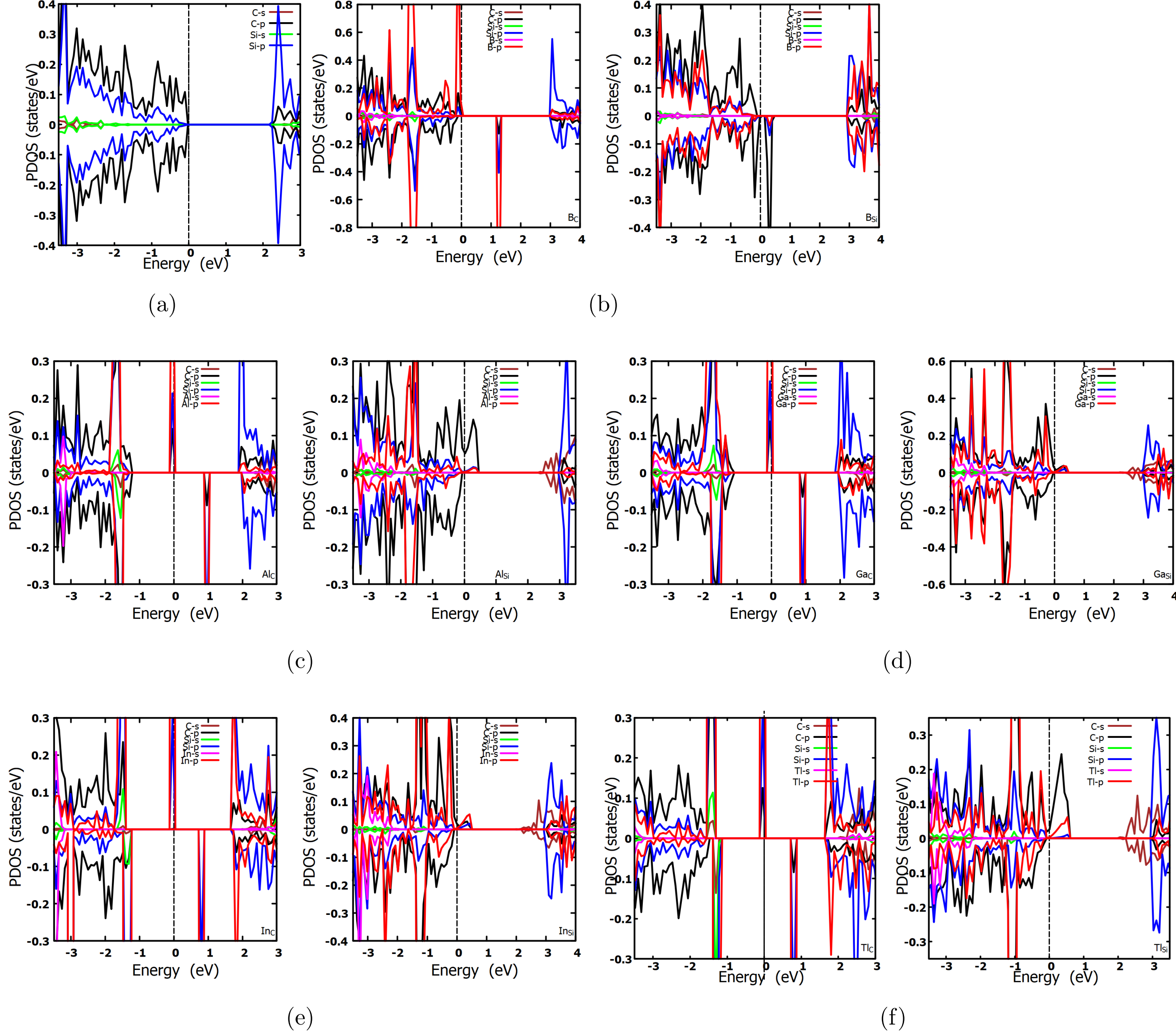

Figure 4: The plots of the PDOS for the (a) Pristine (b) B_C and B_{Si}, (c) Al_C and Al_{Si}, (d) Ga_C and Ga_{Si} (e) In_C and In_{Si} (f) Tl_C and Tl_{Si}. The vertical dash line is the Fermi level, set to zero.

The Al_C induces strong mid-gap states in the host, with the Fermi level located within these states (see Fig 4c). The induced mid-gap states act as traps and can serve as recombination centers. Moreover, Al_C introduces strong spin polarization in the mid-gap region. These states are predominantly contributions from the p orbitals of the participating atoms (Al, Si and C). Due to the large symmetry breakdown, the spin-up component lies at the Fermi level, while one of the spin-down components is shifted by about 1.00 eV above it. In contrast, Al_{Si} does not exhibit sufficient spin polarization, behaving instead as a non-magnetic defect, as will be discussed later. Importantly, the Fermi level of Al_{Si} is pinned to the VBM, consistent with p-type semiconductor behavior. The valence band of the Al_{Si} is densely populated, with only a few induced states near the CBM. This suggests the possibility of electron excitation from the VBM, leaving behind holes. Furthermore, the limited number of states near the CBM indicates reduced electron trapping in the conduction band region. Consequently, Al_{Si} effectively enhances hole concentration, which is beneficial for improving conductivity in semiconductors. The Ga_C, as shown in Figure 4d, induces strong mid-gap states in the host, providing clear evidence of trap states that could lead to recombination centers. The Fermi level of Ga_C is located almost halfway between the VBM and CBM. Furthermore, the band gap of the host is reduced due to the induced mid-gap states. Strong orbital hybridization was observed for the Ga_C. The Ga_C behaves as a magnetic material, since the spin-up and spin-down states are asymmetrically positioned within the band gap. In contrast, the Ga_{Si} preserves the p-type semiconductor of the 2D monolayer SiC, with its Fermi level pinned directly to the VBM. The introduction of Ga at the Si

site produces fewer induced states in the band gap, and the host maintains a band gap of about 2.80 eV. This suggests that 2D monolayer SiC largely retains its semiconducting nature, preserving its electronic integrity, which is an important characteristic for electronic applications. Ga_{Si} can effectively introduce holes into the valence band without significantly distorting the band gap. Specifically, its Fermi level is strongly populated with orbitals from Ga and C p orbitals, while the CBM is only slightly populated with p orbitals from Si atoms.

In_C induces strong asymmetric mid-gap states, suggesting spin polarization. The Fermi level of In_C lies directly on these mid-gap states as shown in Fig. 4e, which could act as traps and lead to recombination centers. If not properly controlled, this may limit carrier lifetimes and negatively impact device efficiency. However, In_C could be useful in applications where spin-dependent characteristics are essential and can be carefully managed. The VBM and CBM of In_C are sparsely populated by the p orbitals of In and Si atoms. Additionally, In_C reduces the band gap of the host, with multiple orbital states induced within it. In_{Si}, on the other hand, has its Fermi level pinned directly to the VBM, signifying that the material behaves as a p-type semiconductor. This suggests that In atom substitution at the Si-site introduces acceptor-like states, effectively generating holes in the valence band. The VBM of the In_{Si} is densely populated with orbitals from the participating atoms. Furthermore, when doped with In on Si site, the band gap of the 2D monolayer SiC remains well preserved. This minimizes the risk of carrier trapping and the formation of recombination centers, as no significant mid-gap states are induced. Therefore, In_{Si} doping is advanta-

geous for tuning 2D monolayer SiC into a *p*-type semiconductor, making it attractive for electronic applications where minimized trap states are critical. As shown in Figure 4f, Tl_C induces strong mid-gap states. The band gap of the 2D monolayer SiC is reduced. The induced mid-gap states are highly asymmetric, indicating the presence of spin polarization. This suggests potential applications in spintronics devices, where spin-dependent transport is important. Strong orbital hybridization is observed between the participating atoms. Both the CBM and VBM are heavily populated with orbitals from the Tl, Si and C atoms. The mid-gap states primarily originate from the *p* orbitals of Tl and C atoms. In contrast, for Tl_{Si}, the Fermi level is pinned to the VBM, with no significant induced mid-gap states. The VBM of Tl_{Si} is heavily populated, whereas the CBM is sparsely populated. Unlike the Tl_C, the band gap of the 2D monolayer SiC is minimally affected. Tl_{Si} could be useful for engineering *p*-type 2D monolayer SiC semiconductors.

3.5. Magnetic and Electronic Charge Transfer of Dopants in Monolayer 2D SiC

Table 3: The magnetic moment (μ) in Bohr and charge transfer between the impurity atom (X) and its nearest neighbour atom.

X_C	μ_B	e	Dis (Å)	X_{Si}	μ_B	e	Dis (Å)
B_C	1.01	-1.79	0.98	B_{Si}	0.00	1.71	0.41
Al_C	1.07	1.74	0.72	Al_{Si}	0.00	2.17	0.67
Ga_C	1.05	-0.27	1.05	Ga_{Si}	0.00	1.14	0.85
In_C	1.00	-0.25	1.18	In_{Si}	0.00	1.03	1.02
Tl_C	0.94	-0.67	1.24	Tl_{Si}	0.00	0.71	1.11

Table 3 lists the calculated magnetic moments in Bohr magnetons (μ_B), charge transfer (e), and displacement in Å between group III impurity atoms (B, Al, Ga, In, Tl) and their nearest-neighbor C or Si atoms in monolayer 2D SiC. Group III dopants at the C site (X_C) induced magnetic moment of approximately 1.00 μ_B for all dopants. While the B_C defect induces the highest magnetic moment, the Tl_C defect induces the lowest; however, it is still significant enough to alter the magnetic properties of the host monolayer 2D SiC. The magnetic moment characteristics of dopants suggest their potential relevance for spintronics applications. In contrast, the substitution of group III dopant on the Si site results in a non-magnetic state (0.00 μ_B).

To understand the origin of magnetism in group III doped 2D monolayer SiC, we examined the atomic orbitals and magnetic moment contributions of the dopants and their nearest neighboring Si atoms, as listed in Table 4.

Table 4: Atomic orbital populations and magnetic moments for B, Al, Ga, In, and Tl substituted on C lattice sites and their nearest Si (Si_1,Si_2, and Si_3) atoms in 2D monolayer SiC.

System	Atom	s (e)	p (e)	p/s	s (μ_B)	p (μ_B)	Total (μ_B)
B_C	B	0.44	0.81	1.80	0.01	0.12	0.13
	Si_1	0.70	0.93	1.32	0.00	0.00	0.00
	Si_2	0.70	0.92	1.31	0.00	0.00	0.00
	Si_3	0.70	0.93	1.32	0.00	0.00	0.00
Al_C	Al	0.57	0.68	1.21	0.00	0.10	0.10
	Si_1	0.71	0.93	1.32	0.00	0.00	0.00
	Si_2	0.70	0.93	1.32	0.00	0.00	0.00
	Si_3	0.71	0.93	1.32	0.00	0.00	0.00
Ga_C	Ga	0.84	0.96	1.14	0.00	0.13	0.13
	Si_1	0.71	0.93	1.31	0.00	0.00	0.00
	Si_2	1.58	2.43	1.54	0.00	0.00	0.00
	Si_3	1.56	2.44	1.56	0.00	0.00	0.00
In_C	In	0.90	1.07	1.19	0.00	0.12	0.12
	Si_1	0.71	0.93	1.31	0.00	0.00	0.00
	Si_2	0.70	0.93	1.33	0.00	0.00	0.00
	Si_3	0.71	0.93	1.31	0.00	0.00	0.00
Tl_C	Tl	1.08	1.12	1.04	0.00	0.12	0.12
	Si_1	0.71	0.93	1.31	0.00	0.00	0.00
	Si_2	0.71	0.93	1.31	0.00	0.00	0.00
	Si_3	0.71	0.93	1.31	0.00	0.00	0.00

The induced total magnetic moment of 1.01 μ_B in B_C arises primarily from

the B atom. The B atom contributes a partial magnetic moment of 0.13 μ_B, mainly from its p-orbital, while the surrounding Si atoms (Si_1, Si_2, and Si_3) possess zero magnetic moments. The partially filled p-orbital of B introduces spin polarization, consistent with the emergence of a magnetic moment in B substituted on lattice site of C in 2D monolayer SiC. This behavior originates from differences in electronic configuration and hybridization. The B atom, having fewer valence electrons and a partially filled p-orbital, retains an unpaired electron that contributes to the magnetic moment. In contrast, the neighboring Si atoms exhibit a more symmetric s–p electron distribution, resulting in fully paired spins and negligible net magnetism. The higher p/s ratio in B (1.80) compared to Si atoms (1.31–1.32) further indicates enhanced p-character, promoting spin polarization and localization of the magnetic moment. For both Al_C and Ga_C, the magnetic properties are dominated by the dopant atoms. In Al_C, the atomic partial magnetic moment analysis shows that the largest single-site moment is located at the Al atom, with a value of 0.10 μ_B arising primarily from its p-orbital. Several Si atoms exhibit only small magnetic moments (0.01–0.03 μ_B), while the nearest-neighbor Si atoms carry essentially zero spin, confirming that the magnetism originates from the Al dopant, among others. This behavior is as a result of the lower valence electron count and smaller p/s ratio (1.21) of Al, which leaves an unpaired electron in the p-orbital that induces spin polarization. A similar trend is observed in Ga_C, where the total magnetic moment is likewise concentrated on the Ga atom. The Ga contributes approximately 0.13 μ_B, mainly from its partially filled p-orbital, while the surrounding Si atoms (Si_1, Si_2, and Si_3) display negligible magnetic moments (0.00 μ_B), and more distant Si atoms

exhibit only minor partial moments (0.01 μ_B). The magnetism in Ga_C, arises from an unpaired electron in the Ga p-orbital. Although Ga has a slightly lower p/s ratio (1.15) than the neighboring Si atoms (1.31–1.56), it retains sufficient p-character to localize spin and generate the observed magnetic moment. For both Al_C and Ga_C, the surrounding Si atoms form strong sp^3-like covalent bonds with adjacent C atoms, leading to symmetric electron distributions, fully paired spins, and negligible contributions to the net magnetism. The total magnetic moments of In_C (1.00 μ_B) and Tl_C (0.94 μ_B) are predominantly localized on their respective dopant atoms. For both cases, In or Tl contributes approximately 0.12 μ_B, arising mainly from the partially filled p-orbital, as listed in Table 4. The surrounding Si atoms (Si_1, Si_2, and Si_3) exhibit negligible magnetic moments (0.00 μ_B), indicating that the magnetism originates from the dopant site among others. In both In_C and Tl_C, the partially occupied p-orbital of In or Tl atom hosts an unpaired electron that induces spin polarization, giving rise to the observed magnetic moments. Although In and Tl form bonds with the nearby Si atoms, they retain an unpaired valence electron in the p-orbital, which localizes the spin and produces magnetism. Meanwhile, the neighboring Si atoms form strong sp^3-like covalent bonds with adjacent C atoms, leading to symmetric s–p hybridization, fully paired spins, and negligible contributions to the overall magnetic moment.

The spin density distributions shown in Fig. 5, particularly for Al, B, Ga, In, and Tl substituted at the C lattice site, reveal that the induced magnetism is highly localized around the impurity atoms. Only very weak contributions are observed on the nearest-neighbor Si atoms, with little spin polarization

extending to other surrounding atoms. For instance, the dominant magnetic moments of B_C, Al_C, Ga_C, In_C, and Tl_C are primarily carried by the p-orbitals of the B, Al, Ga, In and Tl, respectively. Very interesting observation is that the spin polarization decays rapidly beyond the first and second nearest-neighbor atoms to the dopant, confirming the strongly localized nature of the induced magnetism. This localization correlates strongly with p-p orbital hybridization between the dopant and neighboring Si atoms, which mediates the magnetic interaction and governs the spatial extent of the spin density. The dopant p-orbitals hybridize strongly with the p-orbitals of adjacent Si atoms, thereby driving spin polarization in the immediate vicinity.

To further understand their interaction with the host lattice, we conducted a charge transfer analysis to determine how the substitutional atoms donate or accept electrons from their nearest neighboring atoms. Fig 5 shows the plot of the spin-density of substituted group III dopants in 2D monolayer SiC.

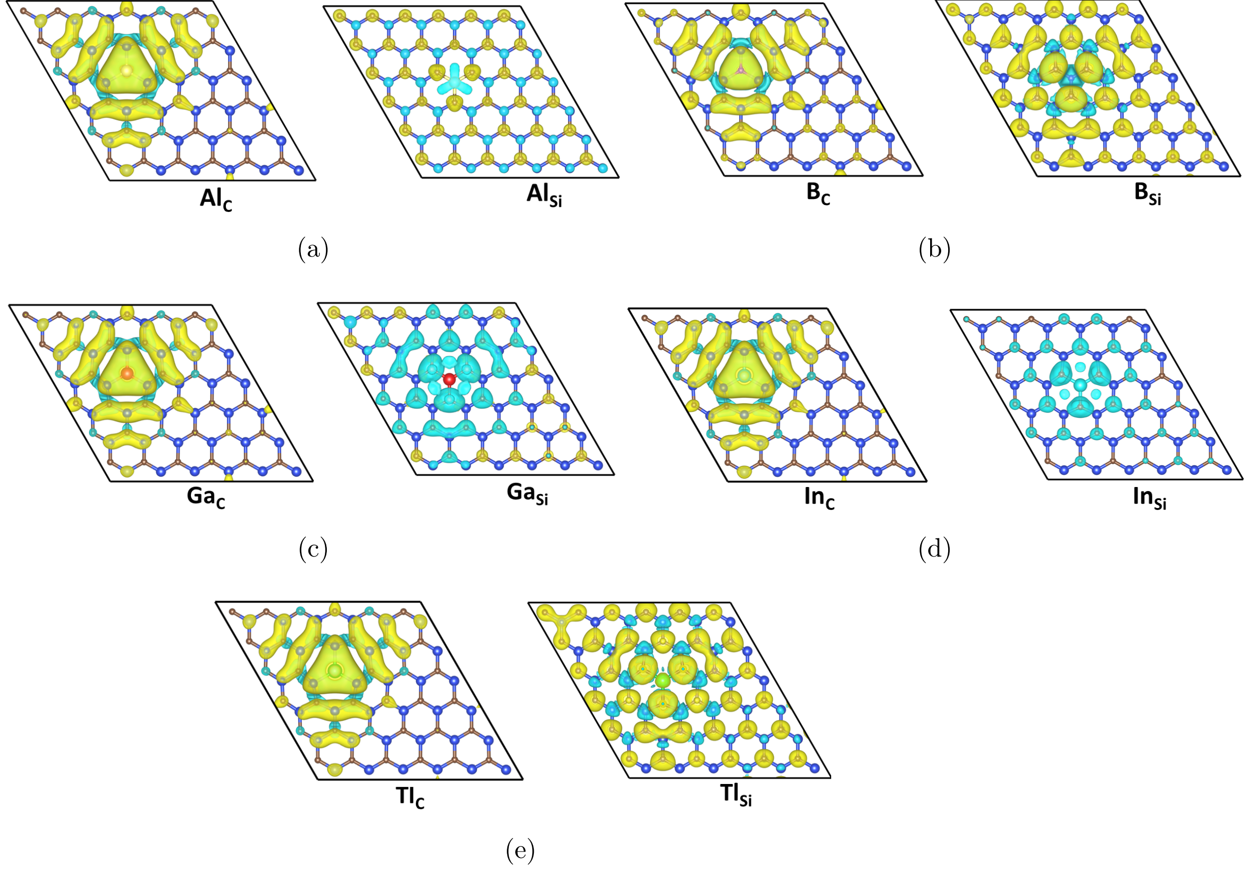

Figure 5: The spin-density plots for group-III substitutions in the 2D SiC monolayer: (a) Al, (b) B, (c) Ga, (d) In, (e) Tl. The yellow regions represent positive spin density, where spin-up electrons dominate, while the blue regions indicate negative spin density, where spin-down electrons dominate.

Dopants substituted at the C site behave as acceptors, accepting electrons from the nearest Si atom, whereas when placed at the Si site, they donate electrons to the neighboring C atom. In particular, B and Al at the C site exhibit significant charge transfers of 1.79 e and 1.74 e, respectively, which make them the major electron recipients from nearby Si atoms (see Figs 5a

and 5b). However, when B and Al are substituted at the Si site, they donate electrons to their nearest neighboring C atoms, resulting in positive charge transfers. In fact, all dopants at the Si site act as electron donors, exhibiting positive charge transfer values. This donor behavior shows a clear trend of decreasing electron donation strength from Al (2.17 e) to Tl (0.71 e), which aligns with the increasing atomic size and decreasing electronegativity down the group.

We further examine the local distortions caused by the dopants (see Table 3) which provides a mechanistic link between lattice mismatch and defect energetics. Defects at the Si site exhibit lower displacement than those at the C site, particularly for lighter dopants such as B and Al. However, the displacement increases with the atomic radius of the dopant. Dopants with radii significantly larger than those of host atoms can cause substantial local lattice distortion. It is interesting to know that C-site dopants show larger displacements than Si-site dopants, increasing systematically with atomic radius (0.98–1.24 Å for C-site and that of the Si-site 0.41–1.11 Å). The charge transfer between the impurity and neighboring atoms correlates with these distortions, indicating that larger dopants induce both significant local lattice strain and electronic redistribution.

At present, there are no experimental reports on group-III doped 2D monolayer SiC. Therefore, the results presented in this study are theoretical predictions that can guide and benchmark future synthesis and characterization of group-III dope 2D monolayer SiC. While the mechanical stability of pristine 2D monolayer SiC via phonon calculation has been studied [28], the influence of substitutional group-III dopants on elastic properties such

as the in-plane elastic modulus, fracture strength, or phonon stability remains experimentally unexplored. Therefore, understanding how substitutional group-III dopants modify the mechanical properties of 2D monolayer SiC is an important direction for future studies.

4. Summary

Hybrid density functional theory was used to study the impact of B, Al, Ga, In and Tl dopants in monolayer 2D SiC. The structural, electronic, magnetic, and defect concentration properties of the aforementioned dopants in 2D monolayer SiC were predicted. The group III dopants substituted in 2D monolayer SiC modulated the original orderly crystal structure, causing the atoms in the flat 2D layer to experience different degrees of lattice distortion. The B_C is the most energetically favorable under the C-rich condition. However, when substituted on Si-sites (B_{Si}), its formation energy under the Si-rihc condition increases to 0.84 eV. In general, the formation energies increase down the group, regardless of whether the dopants occupy C or S lattice sites. Except for Al, all dopants behave as acceptor when substituted on C-sites. In contrast, when they are substituted on Si sites, they act as donors. In their most favorable chemical growth conditions, the defect concentration shows that the Al_{Si} defect concentration exhibits strong temperature dependence behavior of thermally activated processes. The Al_{Si} on the other hand is significantly active at high temperatures. While the B_C is exothermic and thermodynamically favorable at lower temperatures, the Ga_{Si} is thermodynamically favorable at elevated temperatures. The Ga_C is increasingly dominant due to enhanced thermal activation. The In_{Si} defect exhibits a

pronounced temperature-dependent behavior, with its concentration exponentially increasing as the temperature increases. At low temperatures, B_C is the most probable defect, while at high temperatures, Ga_{Si} dominates and is the most thermodynamically favorable. In contrast, In_C, Tl_C, and Tl_{Si} are the least likely to form under equilibrium conditions. Dopants substituted on Si-lattice sites behave as non-magnetic materials. The B, Al, Ga, In, and Tl when substituted at the C lattice sites are good candidates for spin-dependent power electronic devices, as they induce varying degrees of magnetic moments in the host 2D monolayer SiC material. The results of this study are crucial as they provide useful information for the experimental synthesis of group III dopants in 2D monolayer SiC. Furthermore, our results offer valuable insights into defect control in 2D monolayer SiC, which could be beneficial for applications in high-power electronic devices. Furthermore, the results of this study provide theoretical insight that can inform and support future experimental synthesis of group III-doped 2D monolayer SiC. In the future, we will focus on evaluating the ionization energies and defect levels induced by group II dopants in 2D monolayer SiC through charged-defect calculations. Furthermore, detailed studies on lattice strain, phonon dispersion, and related mechanical properties will be addressed in future work.

5. Acknowledgment

Emmanuel Igumbor gratefully acknowledges the University of Johannesburg, South Africa, for funding support. Patience Ajeh thanks the African University of Science and Technology, Abuja, for enabling this research. Edwin Mapasha acknowledges the University of Pretoria for providing compu-

tational resources. The authors appreciate the Center for High Performance Computing (CHPC) Cape Town, South Africa, for providing computational resources

References

[1] C. G. Rodrigues, Electron mobility in bulk n-doped sic-polytypes 3 c-sic, 4 h-sic, and 6 h-sic: A comparison, Semiconductors 55 (2021) 625–632.

[2] E. Igumbor, O. Olaniyan, R. E. Mapasha, H. T. Danga, E. Omotoso, W. E. Meyer, Electrically active induced energy levels and metastability of b and n vacancy-complexes in 4h–sic, Journal of Physics: Condensed Matter 30 (2018) 185702.

[3] S. Guernoub, I. Touati, A. Khoualdia, H.-e. Doghmane, A. Doghmane, Quantification of the impact of hexagonal percentage on the elastic and acoustic properties of sic polytypes (3c, 10h, 8h, 6h and 4h), Silicon (2025) 1–12.

[4] W. Lin, Z. Hu, Y. Chen, Y. Zhang, Y. Yu, X. Xu, J. Zhang, Comparison of vibration-assisted scratch characteristics of sic polytypes (3c-, 4h-and 6h-sic), Micromachines 13 (2022) 640.

[5] I. Capan, Electrically active defects in 3c, 4h, and 6h silicon carbide polytypes: A review, Crystals 15 (2025) 255.

[6] V. Gora, F. Auret, H. Danga, S. Tunhuma, C. Nyamhere, E. Igumbor, A. Chawanda, Barrier height inhomogeneities on pd/n-4h-sic schottky

diodes in a wide temperature range, Materials Science and Engineering: B 247 (2019) 114370.

[7] E. Omotoso, W. Meyer, P. J. van Rensburg, E. Igumbor, S. Tunhuma, P. Ngoepe, H. Danga, F. Auret, The effects of high-energy proton irradiation on the electrical characteristics of au/ni/4h-sic schottky barrier diodes, Nuclear Instruments and Methods in Physics Research Section B: Beam Interactions with Materials and Atoms 409 (2017) 241–245.

[8] Y. Wen, Y. Yang, Y. Li, A novel short-circuit protection scheme for silicon carbide (sic) mosfet module considering operation temperature, IEEE Transactions on Power Electronics (2025).

[9] X. Yang, R. Liu, B. Liu, M. Liu, Synthesis of ultra-thin two-dimensional sic using the cvd method, Energies 15 (2022) 6351.

[10] S. Chabi, K. Kadel, Two-dimensional silicon carbide: emerging direct band gap semiconductor, Nanomaterials 10 (2020) 2226.

[11] O. Olaniyan, R. Maphasha, M. Madito, A. Khaleed, E. Igumbor, N. Manyala, A systematic study of the stability, electronic and optical properties of beryllium and nitrogen co-doped graphene, Carbon 129 (2018) 207–227.

[12] O. Olaniyan, E. Igumbor, A. Khaleed, A. Mirghni, N. Manyala, Ab-initio study of the optical properties of beryllium-sulphur co-doped graphene, AIP Advances 9 (2019).

[13] S. Huo, F. Meng, Z. Zhang, Y. Xie, X. Hu, E. Wu, Bias voltage-switchable metal-insulator transition in 2d van der waals tmds fets: Role of tunneling barriers, Nano Research (2025).

[14] A. Razaq, F. Bibi, X. Zheng, R. Papadakis, S. H. M. Jafri, H. Li, Review on graphene-, graphene oxide-, reduced graphene oxide-based flexible composites: From fabrication to applications, Materials 15 (2022) 1012.

[15] A. R. Urade, I. Lahiri, K. Suresh, Graphene properties, synthesis and applications: a review, Jom 75 (2023) 614–630.

[16] X. Li, H. Zhu, Two-dimensional mos2: Properties, preparation, and applications, Journal of Materiomics 1 (2015) 33–44.

[17] Z. Li, X. Meng, Z. Zhang, Recent development on mos2-based photocatalysis: A review, Journal of Photochemistry and Photobiology C: Photochemistry Reviews 35 (2018) 39–55.

[18] A. Eftekhari, Tungsten dichalcogenides (ws 2, wse 2, and wte 2): materials chemistry and applications, Journal of Materials Chemistry A 5 (2017) 18299–18325.

[19] A. C. Da Silva, N. A. Caturello, R. Besse, M. P. Lima, J. L. Da Silva, Edge, size, and shape effects on ws 2, wse 2, and wte 2 nanoflake stability: design principles from an ab initio investigation, Physical Chemistry Chemical Physics 21 (2019) 23076–23084.

[20] H. Gao, Y. Fang, Y. Zhou, F. Zheng, T.-Y. Lü, X. Cao, Z.-z. Zhu, S. Wu, Tunable magnetic and electronic properties of crs 2/vs 2 lateral superlattices, Nanoscale 17 (2025) 1592–1601.

[21] H. L. Zhuang, M. D. Johannes, M. N. Blonsky, R. G. Hennig, Computational prediction and characterization of single-layer crs2, Applied Physics Letters 104 (2014).

[22] A. E. Naclerio, P. R. Kidambi, A review of scalable hexagonal boron nitride (h-bn) synthesis for present and future applications, Advanced Materials 35 (2023) 2207374.

[23] R. Mapasha, E. Igumbor, N. Chetty, A hybrid density functional study of silicon and phosphorus doped hexagonal boron nitride monolayer, volume 759, IOP Publishing, 2016, p. 012042.

[24] R. Mapasha, E. Igumbor, N. Andriambelaza, N. Chetty, Electronic properties of b and al doped graphane: A hybrid density functional study, Physica B: Condensed Matter 535 (2018) 287–292.

[25] X. Lin, S. Lin, Y. Xu, A. A. Hakro, T. Hasan, B. Zhang, B. Yu, J. Luo, E. Li, H. Chen, Ab initio study of electronic and optical behavior of two-dimensional silicon carbide, Journal of Materials Chemistry C 1 (2013) 2131–2135.

[26] M. Guo, Z. Cui, T. Zhao, Electronic behavior of organic molecules adsorbed on monolayer sic, Materials Today Communications 39 (2024) 109021.

[27] D. Hoat, M. Naseri, N. N. Hieu, R. Ponce-Pérez, J. Rivas-Silva, G. H. Cocoletzi, Transition from indirect to direct band gap in sic monolayer by chemical functionalization: A first principles study, Superlattices and Microstructures 137 (2020) 106320.

[28] M. Manju, K. Ajith, V. MC, Strain induced anisotropic mechanical and electronic properties of 2d-sic, Mechanics of Materials 120 (2018) 43–52.

[29] Q. Wang, R. Luo, Y. Wang, W. Fang, L. Jiang, Y. Liu, R. Wang, L. Dai, J. Zhao, J. Bi, et al., Set/reset bilaterally controllable resistance switching ga-doped ge2sb2te5 long-term electronic synapses for neuromorphic computing, Advanced Functional Materials 33 (2023) 2213296.

[30] Z. Li, S. Zhou, Gaussian-based analytical model for temperature-dependent iv characteristics of gan hemts, IEEE Journal of the Electron Devices Society (2025).

[31] E. Omotoso, A. Paradzah, P. J. van Rensburg, M. Legodi, F. Auret, E. Igumbor, H. Danga, M. Diale, W. Meyer, Electrical characterisation of deep level defects created by bombarding the n-type 4h-sic with 1.8 mev protons, Surface and Coatings Technology 355 (2018) 2–6.

[32] E. Igumbor, O. Olaniyan, R. E. Mapasha, H. T. Danga, E. Omotoso, W. E. Meyer, Induced defect levels of p and al vacancy-complexes in 4h-sic: A hybrid functional study, Materials Science in Semiconductor Processing 89 (2019) 77–84.

[33] E. Igumbor, G. Dongho-Nguimdo, R. Mapasha, E. Omotoso, W. Meyer, Stability, electronic and defect levels induced by substitution of al and p pair in 4h–sic, Journal of Physics and Chemistry of Solids 142 (2020) 109448.

[34] E. Igumbor, H. T. Danga, E. Omotoso, W. E. Meyer, Defect levels induced by double substitution of b and n in 4h-sic, Nuclear Instruments

and Methods in Physics Research Section B: Beam Interactions with Materials and Atoms 442 (2019) 41–46.

[35] Z. Wu, Y. Wang, Y. Dou, L. Zhou, J. Zhu, Property modulations of two-dimensional materials under compression, Nano research energy 2 (2023) e9120080–e9120080.

[36] P. Gong, Y.-Y. Yang, W.-D. Ma, X.-Y. Fang, X.-L. Jing, M.-S. Cao, Theoretical studies on the optical properties of group-iii elements doped sicnts, Optical Materials 117 (2021) 111148.

[37] B. Onat, L. Hallioglu, S. Ipek, E. Durgun, Tuning electronic properties of monolayer hexagonal boron phosphide with group iii–iv–v dopants, The Journal of Physical Chemistry C 121 (2017) 4583–4592.

[38] T. U. Nærland, S. Bernardini, N. Stoddard, E. Good, A. Augusto, M. Bertoni, Comparison of iron-related recombination centers in boron, gallium, and indium doped silicon analyzed by defect parameter contour mapping, Energy Procedia 124 (2017) 138–145.

[39] A. Gökçe, E. Aktürk, A first-principles study of n-type and p-type doping of germanium carbide sheet, Applied Surface Science 332 (2015) 147–151.

[40] E. Igumbor, G. Dongho-Nguimdo, R. Mapasha, W. Meyer, Electronic properties and defect levels induced by group iii substitution–interstitial complexes in ge, Journal of Materials Science 54 (2019) 10798–10808.

[41] L. Lu, H. Zhang, X. Wu, J. Shi, Y.-Y. Sun, Atomic and electronic

structures of p-type dopants in 4h-sic, Chinese Physics B 30 (2021) 096806.

[42] B. Aradi, A. Gali, P. Deák, N. Son, E. Janzén, Passivation of p-type dopants in 4h-sic by hydrogen, Physica B: Condensed Matter 308 (2001) 722–725.

[43] H. Huang, J. Peng, H. Dong, L. Huang, M. Wen, F. Wu, A first principles study of p-type doping in two dimensional gan, Physical Chemistry Chemical Physics 23 (2021) 20901–20908.

[44] C. Persson, U. Lindefelt, B. Sernelius, Band gap narrowing in n-type and p-type 3c-, 2h-, 4h-, 6h-sic, and si, Journal of applied physics 86 (1999) 4419–4427.

[45] P. Gong, Y.-J. Li, Y.-H. Jia, Y.-L. Li, S.-L. Li, X.-Y. Fang, M.-S. Cao, Comparative study on transport properties and scattering mechanism of group iii doped sic nanotube, Physics letters A 382 (2018) 2484–2488.

[46] U. Grossner, J. Furthmüller, F. Bechstedt, Stability, reconstruction, and surface electronic states of group-iii atoms on sic (111), Physical Review B 64 (2001) 165308.

[47] E. M. Handy, M. V. Rao, O. Holland, P. Chi, K. Jones, M. Derenge, R. Vispute, T. Venkatesan, Al, b, and ga ion-implantation doping of sic, Journal of electronic materials 29 (2000) 1340–1345.

[48] F. De Santiago, A. Trejo, A. Miranda, F. Salazar, E. Carvajal, L. Pérez, M. Cruz-Irisson, Carbon monoxide sensing properties of b-, al-and ga-doped si nanowires, Nanotechnology 29 (2018) 204001.

[49] M. M. Haque, S. M. Choudhury, Tailoring electronic and optoelectronic properties of 2d-sic via defects and doping: a first-principles study toward efficient white light-emitting diodes, RSC advances 15 (2025) 29335–29366.

[50] G. Kresse, D. Joubert, From ultrasoft pseudopotentials to the projector augmented-wave method, Physical review b 59 (1999) 1758.

[51] J. P. Perdew, K. Burke, M. Ernzerhof, Generalized gradient approximation made simple, Physical review letters 77 (1996) 3865.

[52] J. Heyd, G. E. Scuseria, Efficient hybrid density functional calculations in solids: Assessment of the heyd–scuseria–ernzerhof screened coulomb hybrid functional, The Journal of chemical physics 121 (2004) 1187–1192.

[53] N. Ferdous, M. S. Islam, J. Biney, C. Stampfl, J. Park, Two-dimensional sic/aln based type-ii van der waals heterobilayer as a promising photocatalyst for overall water disassociation, Scientific Reports 12 (2022) 20106.

[54] S. Chabi, Z. Guler, A. J. Brearley, A. D. Benavidez, T. S. Luk, The creation of true two-dimensional silicon carbide, Nanomaterials 11 (2021) 1799.

[55] L. Huang, H. Liu, X. Deng, W. Cui, The structural, mechanical and electrical properties of 2d sic with c-related point defects and substitution of c by foreign atoms, Vacuum 208 (2023) 111700.

[56] A. Singh, V. Mahamiya, A. Shukla, Defect-driven tunable electronic and optical properties of two-dimensional silicon carbide, Physical Review B 108 (2023) 235311.

[57] K. Sueoka, E. Kamiyama, J. Vanhellemont, Density functional theory study on the impact of heavy doping on si intrinsic point defect properties and implications for single crystal growth from a melt, Journal of Applied Physics 114 (2013).

[58] F. Lee, M. Tripathi, R. S. Salas, S. P. Ogilvie, A. A. Graf, I. Jurewicz, A. B. Dalton, Localised strain and doping of 2d materials, Nanoscale 15 (2023) 7227–7248.

[59] C. Ahn, N. Bennett, S. T. Dunham, N. E. Cowern, Stress effects on impurity solubility in crystalline materials: A general model and density-functional calculations for dopants in silicon, Physical Review B—Condensed Matter and Materials Physics 79 (2009) 073201.

[60] J. Zhu, F. Liu, G. Stringfellow, S.-H. Wei, Strain-enhanced doping in semiconductors: effects of dopant size and charge state, Physical review letters 105 (2010) 195503.

[61] C. Deger, S. Tan, K. Houk, Y. Yang, I. Yavuz, Lattice strain suppresses point defect formation in halide perovskites, Nano Research 15 (2022) 5746–5751.

[62] A. Wu, Q. Song, L. Yang, Q. Hao, The stability and electronic structures of b or/and n doped sic nanotubes: a first-principles study, Computational and Theoretical Chemistry 977 (2011) 92–96.

[63] L. Yu, H. Jin, D. Liu, Y. Dai, M. Guo, B. Huang, Z. Zhang, Investigation of ferromagnetism in al-doped 4h–sic by density functional theory, Chemical Physics Letters 496 (2010) 276–279.

[64] M. Ghezellou, P. Kumar, M. E. Bathen, R. Karsthof, E. Ö. Sveinbjörnsson, U. Grossner, J. P. Bergman, L. Vines, J. Ul-Hassan, The role of boron related defects in limiting charge carrier lifetime in 4h–sic epitaxial layers, APL Materials 11 (2023).

[65] K. Rüschenschmidt, H. Bracht, M. Laube, N. Stolwijk, G. Pensl, Diffusion of boron in silicon carbide, Physica B: Condensed Matter 308 (2001) 734–737.

[66] T. Knezevic, E. Jelavić, Y. Yamazaki, T. Ohshima, T. Makino, I. Capan, Boron-related defects in n-type 4h-sic schottky barrier diodes, Materials 16 (2023) 3347.

[67] Y. Wang, H. Lan, Q. Shangguan, Y. Lv, C. Jiang, A multiscale simulation on aluminum ion implantation-induced defects in 4h-sic mosfets., Electronics (2079-9292) 13 (2024).

[68] V. Heera, D. Panknin, W. Skorupa, p-type doping of sic by high dose al implantation—problems and progress, Applied Surface Science 184 (2001) 307–316.

[69] T. Kimoto, J. A. Cooper, Fundamentals of silicon carbide technology: growth, characterization, devices and applications, John Wiley & Sons, 2014.

[70] N. Saks, A. Suvorov, D. Capell, High temperature high-dose implantation of aluminum in 4h-sic, Applied physics letters 84 (2004) 5195–5197.

[71] S. Smith, A. Evwaraye, W. Mitchel, M. Capano, Shallow acceptor levels in 4h-and 6h-sic, Journal of electronic materials 28 (1999) 190–195.

[72] M. Spera, D. Corso, S. Di Franco, G. Greco, A. Severino, P. Fiorenza, F. Giannazzo, F. Roccaforte, Effect of high temperature annealing (t$>$ 1650 c) on the morphological and electrical properties of p-type implanted 4h-sic layers, Materials Science in Semiconductor Processing 93 (2019) 274–279.

[73] G. Alfieri, L. Knoll, L. Kranz, R. Minamisawa, V. Sundaramoorthy, Point defects in ga-implanted sic: Experiment and theory, Journal of Applied Physics 121 (2017).

[74] Y. A. Vodakov, G. Lomakina, E. Mokhov, E. Radovanova, V. Sokolov, M. Usmanova, G. Yuldashev, B. Machmudov, Silicon carbide doped with gallium, physica status solidi (a) 35 (1976) 37–42.

[75] R. Nipoti, H. M. Ayedh, B. G. Svensson, Defects related to electrical doping of 4h-sic by ion implantation, Materials Science in Semiconductor Processing 78 (2018) 13–21.

[76] M. H. Tehrani, E. Companys, A. Dago, J. Puy, J. Galceran, New methodology to measure low free indium (iii) concentrations based on the determination of the lability degree of indium complexes. assessment of in (oh) 3 solubility product, Journal of Electroanalytical Chemistry 847 (2019) 113185.

[77] Z. Gao, Ultra-Near-Surface Gallium-Activated 435nm Luminescence from Donor-Acceptor-Pair Recombination in Ion-Beam Implanted 4h Sic, Ph.D. thesis, 2025.

[78] L. Huang, L. Gu, H. Liu, X. Zhai, X. Gu, J. Wang, Tunable electrical and magnetic properties of 2d sic via adsorption and doping of atmospheric elements (h, c, n, and o), Physica B: Condensed Matter 679 (2024) 415809.